Copper-nickel mixed oxide catalysts from layered double hydroxides for the hydrogen-transfer valorisation of lignin in organosolv pulping

Copper-nickel mixed oxide catalysts from layered double hydroxides for the hydrogen-transfer valorisation of lignin in organosolv pulping.

Iqra Zubair AWAN,[a,b,1] Giada BELTRAMI,[c] Danilo BONINCONTRO,[a,2] Olinda GIMELLO,[b] Thomas CACCIAGUERRA,[b] Nathalie TANCHOUX,[b] Annalisa MARTUCCI,[c] Stefania ALBONETTI,[a] Fabrizio CAVANI,[a] Francesco DI RENZO[b,*]

[a] Department of Industrial Chemistry Toso-Montanari, Alma Mater Studiorum Università di Bologna, Viale Risorgimento 4, 40136 Bologna, Italy

[b] ICGM, Univ Montpellier-CNRS-ENSCM, 240 Avenue Emile Jeanbrau, 34296 Montpellier, France

[c] Department of Physics and Earth Sciences, University of Ferrara, Via Saragat 1, 44100 Ferrara, Italy

Keywords

Heterogeneous catalysis; lignin depolymerisation; catalytic transfer hydrogenation; hydrotalcite; in-situ activation

Abstract

Copper and nickel mixed catalysts obtained by calcination of iron and aluminium hydrotalcites (layered double hydroxides, LDH) have been tested in the conversion of a lignin model dimer in subcritical methanol. The phase distribution and the textural properties of the catalysts have been characterized by X-ray diffraction Rietveld analysis and N_2 physisorption. The presence of copper was critical for effective hydrogenation, both by direct hydrogen transfer from methanol to aldehyde groups and by the reactivity of products from methanol reforming. The presence of mixed oxides in the catalysts highly promoted the hydrogenation activity. TPR experiments showed that the hydrogenation activity was related to an enhanced reducibility of the catalysts. Characterisation of the catalysts after reaction indicated that metallic copper was formed from

---

[1] Present address: Department of Polymer Engineering and Technology, University of the Punjab, New Campus, Lahore, Pakistan

[2] Present address: D. Bonincontro, Department of Energy, Politecnico di Milano, Milano, Italy

* Corresponding author: F. Di Renzo, ICGM, Univ Montpellier-CNRS-ENSCM, 240 Avenue Emile Jeanbrau, 34296 Montpellier, France. direnzo@enscm.fr. tel. +33 607508148.

reduction of CuO by methanol and that modifications of the oxide catalysts in the reaction medium played a major role in the formation of active sites. The absence of Mg-related strong basic functions in the catalysts has allowed to isolate and highlight the effects of solvolysis and hydrogen transfer reactions in organosolv treatments. NiO catalysts favoured the solvolysis of phenyl ether bonds by phenyl-methyl transetherification. The mild acidity of amorphous alumina promoted the protection of aldehyde groups by acetalisation.

1. Introduction

The perspective of economical valorisation of all components of lignocellulosic biomass in chemicals and fuels is at the basis of the development of more advanced processes, leading to integrated biorefineries [1-6].[1,2,3.4,5,6] Among the processes aiming at coping with the specifications of new market flows, organosolv pulping has received a renewed interest. [7, 8][7,8] The use of organic solvents in pulping process, allowing an efficient recovery of the lignin fraction of lignocellulosic biomass, has always been a niche industrial reality, due to the competition of fossil-derived products on the market of lignin-derived molecules. The implementation of second generation ethanol plants has opened a new window of opportunity for organosolv treatments, in which the added value of lignin extraction is boosted by the production of valuable easily-fermentable cellulose [9-11].[9,10,11]

Hydrogen-donor solvents used in organosolv processes do not only break lignin-holocellulose bonds and solubilize lignin but also represent an appropriate source of hydrogenating reagents, able to stabilize lignin fragments towards unwanted re-condensation. Indeed, the processes of valorisation of lignin through depolymerisation to market chemicals have always been plagued by the easy formation of heavy recalcitrant compounds by condensation of lignin fragments [12-14].[12,13,14] The classical view of the mechanisms of re-condensation of lignin fragments implied the formation of diphenylmethane-type bonds by Michael addition of phenolic carbanions to quinone methide intermediates or the aldol condensation of aldehydes formed by alkaline cleavage of alkylphenyl ethers [15, 16].[15 ,16] More recently, this last condensation pathway has been revisited and integrated with a mechanism of polymerisation of the reactive aldehydes formed by acidolysis of β-O-4 bonds, the most frequent linkages in lignin [17].[17] The relevance of this mechanism has been confirmed by the effectiveness of the hydrogenation of aldehydes or the introduction of appropriate end-capping groups in preventing the re-condensation of lignin-derived monomers [18-20].[18,19,20]

The nature of marketable products which can be obtained from organosolv lignin is significantly affected by its level of hydrogenation in the biorefinery process. High hydrogenation in the

pulping process would decrease the burden of further hydrodeoxygenation units in the production of bio-oil or BTX [21-24].[21,22,23,24] However, deep hydrogenation would prevent the preservation of valuable functional groups for fine chemistry applications [25].[25] Among the solvents used in organosolv processes, methanol has been often proposed as a source of hydrogen in biomass-to-fuel processes [26].[26] Methanol in liquid phase is an effective hydrogenating agent, able to go beyond MPV (Meerwein-Ponndorf-Verley) hydrogen exchange with carbonyl groups and providing deeper hydrogenation by generation of hydrogen through disproportionation to formaldehyde and CO [27].[27]

The benefits of heterogeneous catalysis, fully developed in the transformation of fossil resources, are still largely to be exploited in the valorisation of biomass [28].[28] If heterogeneous catalysts are finding useful applications in the chemistry of cellulose-derived molecules, they are at a preliminary stage of development for the fractionation of biomass and the valorisation of lignin [29-335].[29,30,31,32,33,34,35]

Supported Ni catalysts have been shown to be active in the reductive depolymerisation of birch sawdust lignin to monomeric phenols with methanol solvent as only source of hydrogen [36, 37].[36,37] Cu-bearing porous metal oxides (PMO) formed by calcination of layered double hydroxides (LDH) have been presented as effective catalysts for the depolymerisation of lignin in supercritical methanol [38-40].[38,39,40] These materials have also been proved effective in catalytic transfer hydrogenolysis of lignocellulosic biomass, furfural, 5-hydroxymethylfurfural, and ethanol Guerbet reaction to butanol [41-45]. [41,42,43,44,45] Supercritical methanol was often used in previous studies of hydrogen transfer on biomass components [46-48]. [46,47,48] The required levels of temperature and pressure represent conditions more severe than in traditional organosolv pulping in methanol, which generally operate at temperature significantly lower than 220 °C [49],[49] and the need for milder reaction conditions has been acknowledged [50].[50]

The purpose of the present work is the evaluation of a series of mixed oxide catalysts in the conversion of a lignin model molecule by hydrogen transfer from methanol. Reaction conditions well below the critical point of methanol have been chosen, namely 200 °C and autogenous pressure from methanol at this temperature, in order to stay near temperature and pressure compatible with known organosolv processes. The addition of acid or bases has been avoided, as well as the use of highly basic magnesium-bearing materials, in order to isolate and better understand the effects of hydrogen transfer from the solvent to the model lignin moiety. The relative effect of Cu and Ni cations in the catalysts has been studied. Beyond the usual aluminium-based LDH, iron-bearing materials have been tested, as they present a potential

interest in the magnetic separation of the catalyst from the complex mixture of products of an organosolv pulping process [51, 52].[51,52]

2. Experimental

2.1. Preparation and characterization of catalysts

Precursors of the catalysts were prepared by addition of sodium carbonate solutions to nitrate solutions of the metal cations in the appropriate ratios, keeping constant pH 10. Hydrotalcite-type layered double hydroxides were formed in the Cu-Ni-Fe and Cu-Ni-Al systems, accompanied by CuO tenorite in copper-rich samples. Single-cation materials were prepared as reference by the same procedure. These precursors were dried at 80 °C and calcined at 600 °C under air flow. The catalysts are named by their composition as, for instance, Cu4Ni72Fe26, where the numbers following the element symbols indicate the atomic fractions of the cations in percent.

The catalysts were characterized by EDX analysis, powder X-ray diffraction with Rietveld phase analysis, N_2 sorption and H_2-TPR. X-ray powder diffraction (XRD) patterns were measured using a Bruker D8 Advance Bragg-Brentano diffractometer equipped with a Si(Li) solid state detector (SOL-X) and a sealed tube providing Cu K radiation (copper anode, 40 kV and 40 mA). Apertures of divergence, receiving, and detector slits were 2.0 mm, 2.0 mm, and 0.2 mm, respectively. Data scans were performed in the 2θ range 5–75 ° with 0.02 °2θ, 1.06 s per step. The refinements for the quantitative phase analyses (QPA) were performed using the GSAS package and its graphical interface EXPGUI [53, 54].[53,54] The weight percentages were calculated from the scale factors, unit cell masses, and unit cell volumes of the constituent phases according to the equation:

$$W_\alpha = \frac{S_\alpha \ (ZMV)_\alpha}{\sum_{k=1}^{n} S_k \ (ZMV)_k}$$

where Wα = weight fraction of phase α in an n component mixture, S = Rietveld scale factor, ZMV = mass and volume of unit cell [55-57].[55,56,57]

Structural models for crystalline phases were taken from the ICSD database. Depending upon the number of catalyst phases, the refined variables ranged up to 42 independent variables including scale factors, zero-point, lattice parameters, 16 coefficients of the shifted Chebyschev function to fit the background. The line shape was described by a pseudo-Voigt function with the

following refinable coefficients: three Gaussian terms (Gu, Gv, Gw), two Lorentzian terms (Lx, Ly), S/L (S: sample size; L: distance between sample and detector) and H/L (H: detector height; L: distance between sample and detector) to account for profile asymmetry due to axial divergence. Site occupancies and atomic displacement parameters were kept fixed in all the stages of Rietveld refinements.

N_2 sorption isotherms at 77 K were measured on a Micromeritics Tristar apparatus with enhanced secondary void system after outgassing overnight at 250 °C. Surface area was determined by the BET method and mesopore distribution by a DFT kernel [58].[58] Micropore volume was measured by the αS method. Crystallite size was measured by the Scherrer method.

TPR (Temperature Programmed Reduction) experiments were performed using a Micromeritics Autochem 2920 equipped with a mass spectrometer MKS Cirrus II to evaluate H_2 consumption. All the tests were carried out by pretreating the samples under He flow (30mL/min) for 30min at 450 °C (heating ramp 10 °C/min). Then, the samples were cooled down to 25 °C, the gas flow was switched to H_2 (5% in He v/v, 30mL/min), and the temperature was increased to 900°C (heating ramp 10°C/min) for the analysis.

2.2. Catalytic tests

20 mg catalysts were introduced in each of six 120 ml autoclaves containing 20 ml of 5mM solution of BMBA in anhydrous methanol. The autoclaves were connected to a Parr 5000 system and deoxygenated by bubbling N_2 in successive cycles of pressurization and depressurization. The closed autoclaves were heated at 5 °C/min and maintained 3h at 200 °C under stirring at 500 rpm. At an autogeneous pressure of 40 atm with 17% autoclave filling, nearly 70% of methanol is in the liquid phase. The liquid products recovered after cooling were identified by GC-MS (Shimadzu GCMS-QP 2010, low polarity polyimide Zebron ZB-5HT column) and quantified by a GC-FID equipped with the same column. Yields of products were calculated as ratios between carbon atoms of each product and carbon atoms of BMBA reagent.

3. Results and discussion

3.1. Phase characterization of catalysts

The catalysts were mixed oxides in the Cu-Ni-Fe and Cu-Ni-Al systems spanning the field of Cu/divalent ratio from 0 to 1, with divalent/trivalent ratio 3. The catalysts were obtained by calcination at 600 °C of the hydroxide or oxyhydroxide precursors. Single-oxide benchmark catalysts presented single phases of NiO bunsenite, CuO tenorite or Fe_2O_3 α-hematite. Their

XRD patterns are shown in Fig. S1. All mixed oxide catalysts presented several crystalline phases, whose ratios, determined by Rietveld method, are shown in Fig. 1 and reported in detail in Tab. S1. XRD patterns are shown in Figures S2 and S3 for, respectively, the Cu-Ni-Fe and Cu-Ni-Al systems. NiO bunsenite and CuO tenorite were the prevalent phases, with their ratio evolving with the Cu/(Cu+Ni) ratio (Fig. 1). A minor spinel phase was present in all Fe-bearing samples. Some information on the composition of spinels is provided by their *a* cell parameter, which in Ni-containing samples varied from 8.34 to 8.36 (Tab. S1), compatible with solid solutions of intermediate composition between $NiFe_2O_4$ (8.32 Å) and Fe_3O_4 magnetite (8.39 Å) [59].[59] In the Ni-free samples, the cell size of spinel was 8.41 Å, between the *a* parameters of magnetite and $CuFe_2O_4$ (8.42 Å) [60].[60] In nearly all Fe-bearing samples, the amount of spinel evaluated from the X-ray diffraction patterns was much lower than the amount of trivalent cation expected from the iron content of the samples. This effect was still more evident in the Al-bearing catalysts, in which CuO and NiO were the only crystalline phases observed and no explicit Al-bearing phase was detected by XRD.

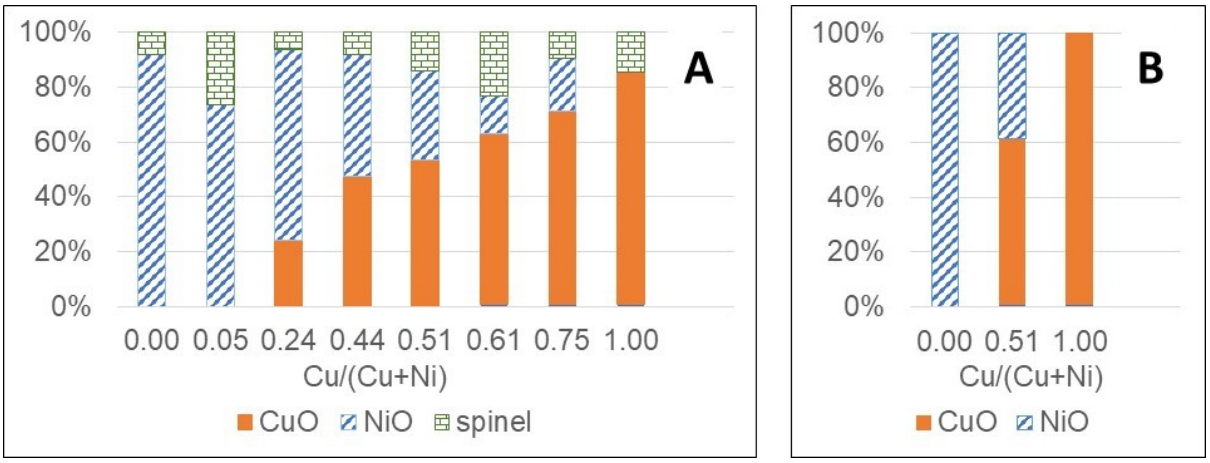

Fig 1. XRD phase composition of the mixed oxide catalysts in the (A) Cu-Ni-Fe and (B) Cu-Ni-Al systems

The incorporation of some Fe and Al in CuO and NiO phases could partially justify the missed or insufficient observation of spinel phases. Indeed, the cell parameters of tenorite and bunsenite in the mixed samples were systematically slightly lower than the parameters of the pure phases (Tab. S1 and S2). A decrease of cell parameter can be attributed to the presence of cation vacancies, corresponding to the incorporation of trivalent cations in the sites of divalent cations [61, 62].[61,62]

However, limited incorporation of trivalent in the divalent oxide phases can only partially justify the low amount of spinel in the XRD patterns of Fe-bearing catalysts and does not justify the complete absence of alumina phases in the Al-bearing catalysts. These effects have to be largely attributed to the presence of trivalent cations in an XRD-amorphous material. Indeed, it has been often shown that mixed hydroxide samples calcined at 600 °C are expected to contain a large amount of trivalent-rich amorphous material. Al-containing spinel phases are observed only for calcination temperature higher than 750 or 850 °C for Ni-Al or Ni,Cu-Al hydrotalcites [63, 64].[63,64]

3.2. Textural characterization of catalysts

The N_2 adsorption-desorption isotherms of the catalysts are reported in Figs. S4-S6. The surface area and the mesopore volume of the mixed oxide catalysts are reported in Fig. 2 as a function of the Cu/(Cu+Ni) ratio. Complete textural data of the catalysts are reported in Tab. S3. The surface area of the Al-bearing catalysts is nearly twice the surface area of the Fe-bearing samples. The increase of the copper content induces a decrease of the surface area in both Fe-bearing and Al-bearing series of catalysts. The surface area of the catalysts varies from 191 to 42 $m^2 g^{-1}$ at the increase of copper content in the Cu-Ni-Al system and from 89 to 25 $m^2 g^{-1}$ in the Cu-Ni-Fe system varies. These variations of the surface area with the composition of the catalysts can be partially accounted for by a corresponding evolution of the crystallite size as measured by the Scherrer method, also reported in Tab. S2. In the Cu-Ni-Fe system, the size of the CuO and spinel crystallites was virtually constant at, respectively, 15.7±1.5 and 8.5±1 nm, independently on the Cu/(Cu+Ni) ratio. The NiO crystallite size, instead, increased from nearly 7 nm for the Cu-free Ni75Fe25 to more than 14 nm for the Cu-rich Cu44Ni28Fe28, contributing to a decrease of the surface area. In the case of the Cu-Ni-Al system, the NiO crystallites were smaller, at 3.8±0.4 nm. The decrease of the amount of NiO with the increase of the Cu/(Cu+Ni) ratio could be a main factor in the decrease of the surface area, despite a decrease of the size of CuO crystallites from 38 nm for Cu30Ni38Al23 to 14 nm for Cu74Al26.

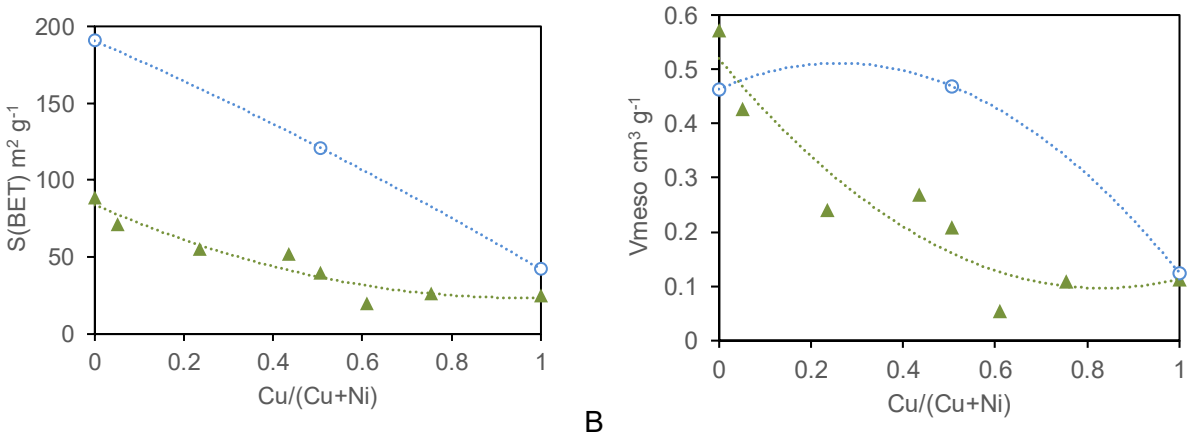

A B

Fig.2. Surface area (A) and mesopore volume (B) of the Fe-bearing (green triangles) and Al-bearing (void circles) catalysts. The lines are a guide for the eye.

The absolute values of experimental surface area do not fully account for the surface areas which would be expected on the basis of the small crystallite sizes measured by the Scherrer method. It is likely that the level of aggregation of nanocrystals plays a significant role in the extent and variations of surface area. It is also likely that the amorphous material present in all samples can contribute to the aggregation of the oxide nanocrystals. Some information on the level of aggregation can be obtained from the measurement of pore size and volume. Moreover, mesoporosity has been considered to be an important property of the lignin degradation catalysts obtained by calcination of hydrotalcites. They have indeed been often referred to as porous metal oxides (PMOs) [38].[38]

The mesopore volume of the catalysts, reported in Fig. 2B, decreases with the increase of the copper content from 0.57 to 0.11 $cm^3\ g^{-1}$ in the Cu-Ni-Fe system and from 0.46 to 0.12 $cm^3\ g^{-1}$ in the Cu-Ni-Al system. The mesopore size (Tab. S3) increases with the copper content from 24 nm for Ni75Fe25 and 12 nm for Ni75Al25 to 35 nm for both Cu65Ni35 and Cu74Ni26. At the increase of copper content, the increase of size of intergranular mesopores parallels the observed decrease of surface area. Both effects are likely related to the presence of larger particles, formed by aggregation of nanocrystallites and amorphous material.

3.3. Thermal-programmed reduction of catalysts

The H_2-TPR curves of the catalysts are reported in fig. 3A. Temperature of onset of decomposition, temperature of the main reduction peaks and fraction of hydrogen consumed in each reduction step are reported In Table 1. The consumption of H_2 in the TPR experiments is reported in Table S4. In the analysis of Ni and Fe containing samples, the evaluation of

hydrogen consumption compared to CuO standard was often higher than the value expected, possibly due to the evolution from the surface of nanocrystals and amorphous oxides of atmospheric water and CO_2 adsorbed after the calcination at 600 °C.

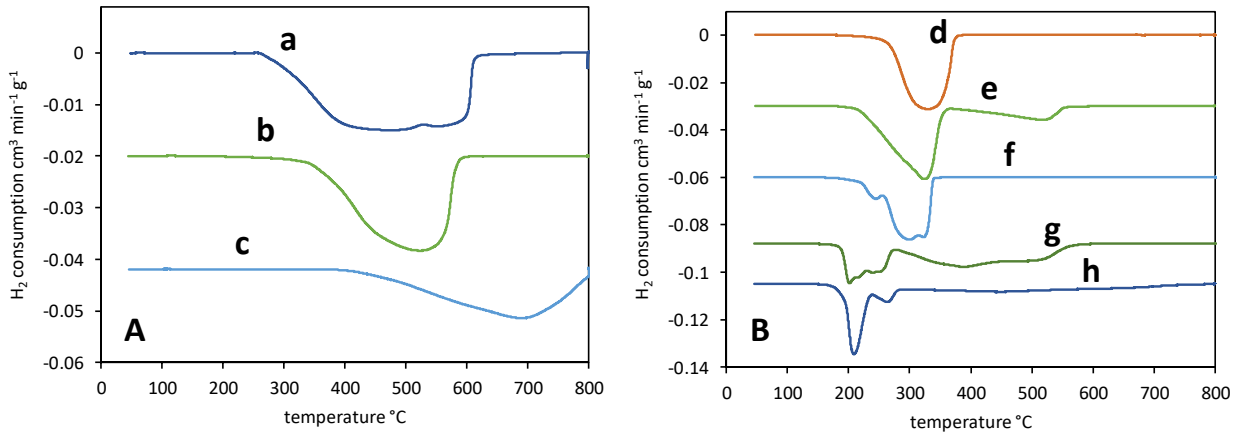

Fig. 3. H_2-TPD curves for (A) Cu-free catalysts, (B) Cu-bearing catalysts: (a) NiO, (b) Ni75Fe25, (c) Ni75Al25, (d) CuO, (e) Cu79Fe21, (f) Cu74Al26, (g) Cu31Ni40Fe29, (h) Cu39Ni38Al23 catalysts.

Table 1. H_2-TPR data: Onset temperature of H_2-TPR reduction; peak temperature and fraction of consumed H_2 of major phenomena.

	onset T	main peaks temperature and corresponding fraction of consumed H_2							
catalyst	°C	°C	H_2 fraction	°C	H_2 fraction	°C	H_2 fraction	°C	H_2 fraction
NiO	265	450	0.75	560	0.25				
Ni75Fe25	345	530	1						
Ni75Al25	415	690	1						
CuO	248	330	1						
Cu79Fe21	215	325	0.79	520	0.21				
Cu74Al26	223	245	0.17	300	0.69	325	0.14		
Cu31Ni40Fe29	181	202	0.22	240	0.13	392	0.47	507	0.18
Cu39Ni38Al23	178	209	0.42	265	0.10	452	0.39	653	0.09

Examining the reduction patterns of the Ni-based Cu-free samples (Fig. 3A), the onset of reduction of NiO was near 250 °C, in good agreement with literature reports for NiO nanoparticles [65].[65] The complex shape of the peak can reflect heterogeneities of crystal size. In the case of Ni75Fe25 catalyst, the reduction began at a higher temperature, 345°C, and presented a maximum at 530 °C. The peak, of complex shape, included the reduction of NiO bunsenite, possibly iron-doped, 8% spinel and perhaps amorphous iron oxides. The reduction of the Ni75Al25 catalyst began at still higher temperature, 415°C, and presented a maximum at 690 °C. This reduction pattern closely followed the trend observed on co-precipitated NiO-Al_2O_3 systems [66].[66]

Cu-bearing catalysts were reduced by H_2 at a lower temperature (Fig. 3B and Table 1). The reduction of CuO started at 248 °C and presented a maximum at 330 °C. Contrarily to what observed in the case of Ni-bearing catalysts, the presence of Fe or Al decreased the reduction temperature. The Cu79Fe21 sample presented a first reduction peak with onset at 215 °C and maximum at 325 °C, including the reduction of CuO and the reduction of Fe^{3+} to Fe^{2+} [67].[67] A second peak, beginning at 375 and with maximum at 520 °C, corresponded to the reduction of the FeO formed in the first reduction step. In the Cu74Al26 sample, CuO reduction followed a complex pattern. A main splitted peak with maxima at 300 and 325 °C is preceded by a small initial peak, beginning at 223 and culminating at 245 °C.

The Cu31Ni40Fe29 sample featured a still lower temperature of onset of reduction, 181 °C. A first composite peak with maxima at 202 and 240 °C consumed the amount of H_2 corresponding to the reduction of CuO to metallic copper. Two following shallower peaks with maxima at 392 and 507 °C merged one into the other. The amount of H_2 consumed in each of the peaks suggested the attribution of the first one to the reduction of NiO and to the partial reduction of spinel to a divalent iron oxide with exsolution of nickel. The last peak would correspond to the reduction of the FeO formed. This pattern of reduction is qualitatively similar to the literature report for TPR of $CuFe_2O_4$, in which a first composite peak with onset at 190 °C was attributed to the reduction of CuO and of divalent copper exsoluted from a cuprospinel, leaving a magnetite Fe_3O_4, which reduction started at about 400 °C [68].[68]

The $Cu_{39}Ni_{38}Al_{23}$ catalyst, in which trivalent Al is not involved in the reduction of the material, featured two initial peaks of H_2 consumption with onset at 178 °C and maxima at 209 and 265 °C. They are followed by two extremely shallow peaks extending from 280 to 800 °C, probably corresponding to the reduction of exsoluted divalent cations from an XRD-amorphous spinel-like

material. In the case of nanocrystalline CuO formed by wet impregnation of γ-Al_2O_3, Yu et al. reported an onset of reduction at 210 °C, lower than the onset temperature of 290 °C for bulk CuO [69]. [69] They also observed that a small fraction of CuO deposited on γ-Al_2O_3 presented a much higher reduction temperature, 410 °C, attributed to interaction with the support.
The granulometry of the oxides did not seem to represent a main factor in the differences of onset temperature of reduction, as the Scherrer grain sizes were 14 nm for both CuO and Cu31Ni40Fe29, and 16-17 nm for both Cu74Al26 and Cu79Fe21 catalysts (Table S3). Admittedly, Scherrer size does not provide information on the size distribution of crystallites and a fraction of smaller, easily-reducible grains can provide early formation of metal, with a catalytic effect on the reduction of larger grains.

3.4. Catalytic activity

3.4.1. Reaction cascade

4-Benzyloxy-3-methoxybenzaldehyde (BMBA) was used as a model dimer of lignin, allowing to study the reactivity of phenolic ether groups, corresponding to the most frequent linkage between monolignols in natural lignin. The presence of an aldehyde group was useful to differentiate the activity of the catalysts in MPV hydrogen transfer and in further hydrogenation, by cleavage of C-O and C-C groups, of the alcohol group formed by hydrogenation of the aldehyde. The main products observed in the catalytic tests and their main reaction pathways are represented in Fig. 4 as a tree of reactions with minor branches of solvolysis and acetalisation on the left side and a complex hydrogenation cascade on the right side. The reactions observed can be classified as (i) solvolysis of the α-O-4 phenyl ether bond by benzyl-methyl transetherification, (ii) etherification of alcohol groups by methanol, (iii) acetalisation of aldehyde groups, (iv) hydrogenation of aldehyde groups by MPV hydrogen transfer, (v) hydrogenolysis of the C-O bond of the benzyl alcohol groups formed, (vi) hydrogenolysis of the C-C bonds of the toluene-like groups formed, (vii) hydrogenolysis of the α-O-4 phenyl ether bonds. The relative and absolute extent at which these reactions are performed strongly depends on the nature of the catalyst.

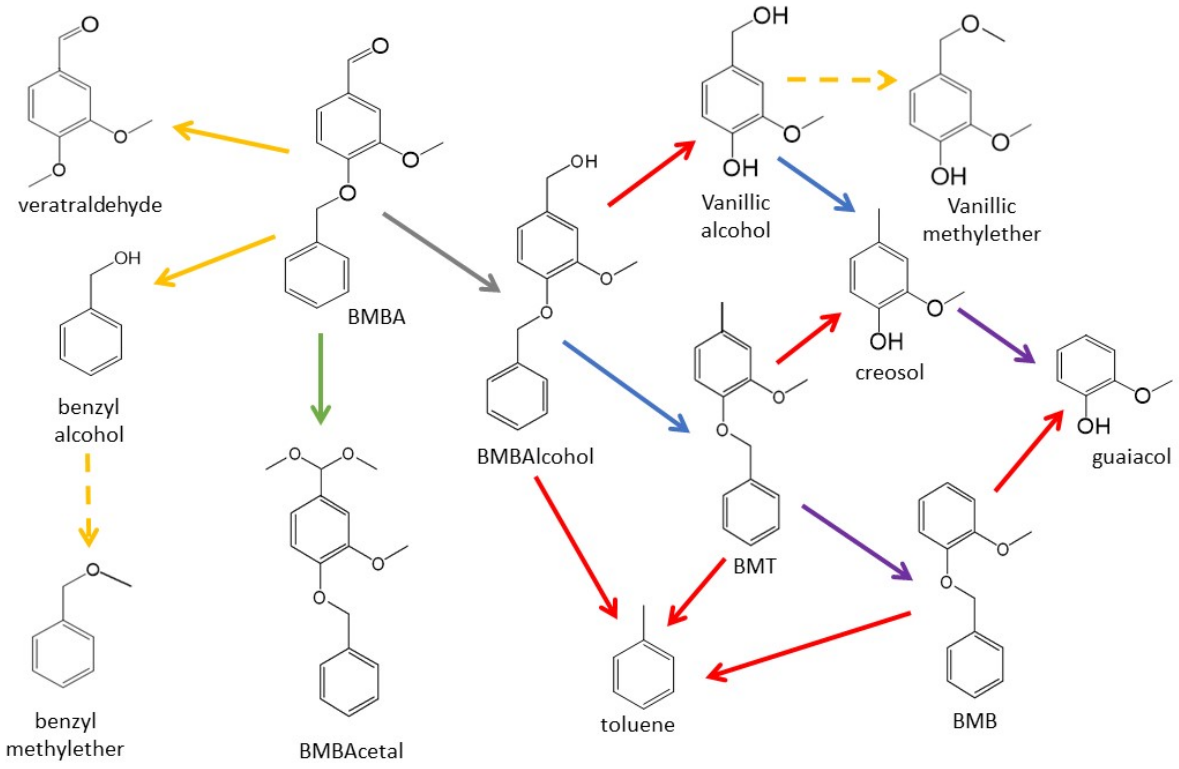

Fig. 4. *Main reaction pathways of BMBA (4-Benzyloxy-3-methoxybenzaldehyde) in methanol. Reaction colour codes: methyl-benzyl transetherification (yellow), methyl etherification of alcohols (dashed yellow), acetalisation (green), MPV aldehyde hydrogenation (grey), C-O hydrogenolysis (blue), C-C hydrogenolysis (violet), α-O-4 hydrogenolysis (red). BMT: 4-benzyloxy-3-methoxy toluene; BMB: 1-Benzyloxy-2-methoxy benzene.*

Blank tests were carried out in the absence of catalyst. The hydrogenation of BMBA in methanol at 200 °C for 3 hours was negligible. However, conversion of 9% BMBA into its methylacetal (BMBAcetal) was observed. No hemiacetal intermediate was observed, probably due to the known unstablility of hemiacetals, which easily revert to the parent alcohol and aldehyde when the equilibrium is shifted.

3.4.2. Single-cation catalysts

The activity of single-cation oxides, *viz.* NiO, CuO and Fe_2O_3, was preliminary studied as a benchmark for the activity of mixed-oxide catalysts prepared and tested in the same conditions. The three single-cation oxides presented quite different reactivity. Conversion of BMBA, carbon balance and yields of the products of different types of reactions are reported in Fig. 5. Detailed results are provided in Table S5. Conversion of BMBA was 20%, 35% and 12%, respectively on

NiO, CuO and Fe_2O_3. These differences in conversion corresponded to very different distributions of products, which will be discussed examining the reactivity of each catalyst.

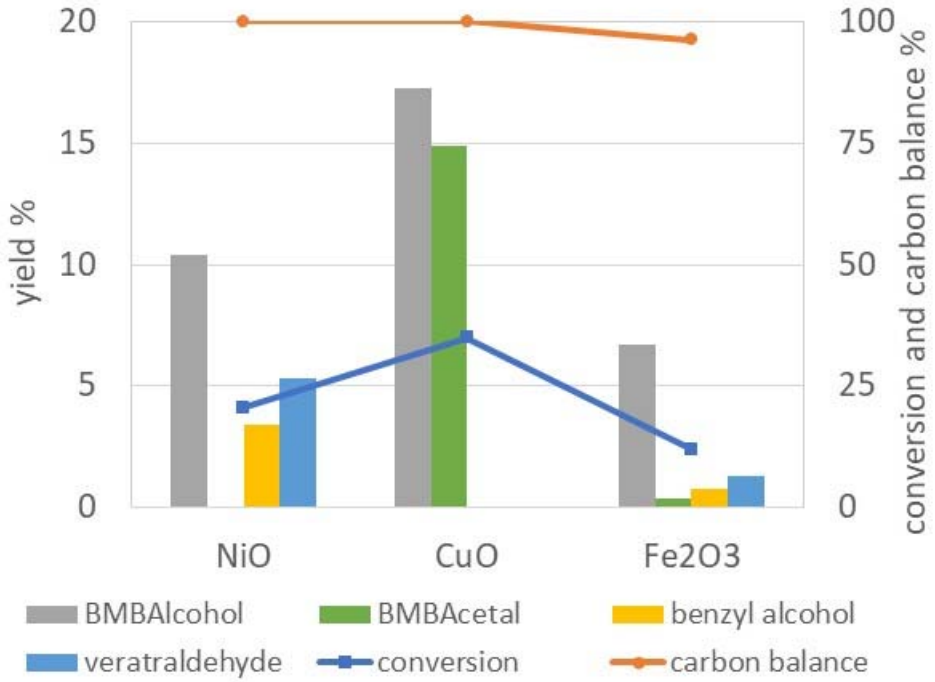

Fig. 5. Conversion, carbon balance and yields of main products of MPV hydrogen exchange (BMBAlcohol), acetalisation (BMBAcetal), and benzyl-methyl exchange (benzyl alcohol and veratraldehyde) on single-cation catalysts.

The main product on NiO was 4-benzyloxy-3-methoxybenzylalcohol (BMBAlcohol), formed by the reaction of MPV hydrogen exchange, with a yield of 10%. Veratraldehyde was formed with a yield of 5%, accompanied by the formation of benzylalcohol and benzylmethylether with a cumulate 4% yield, through a mechanism of transetherification exchange between benzylalcohol and methanol solvent. Solvolysis mechanisms of phenylether bonds by methanol at 250 °C have been reported on Ni/Al_2O_3 catalysts [48].[48] No BMBAcetal was formed in the presence of NiO, despite its significant yield in the blank tests.

CuO catalyst was nearly twice more active than NiO and presented a completely different product distribution (Fig. 5 and Table S5). BMBAlcohol was again the main product, with a yield of 17%, indicating higher activity than NiO in MPV hydrogen exchange. BMBAcetal was present with a yield of 15%, higher than the conversion in the absence of catalyst. Veratraldehyde and benzyl alcohol were negligible.

Products of hydrogenation reactions requiring more severe conditions than the MPV hydrogen

exchange, negligible on NiO, were observed on CuO, allowing for nearly 3% conversion of BMBA (Table S5). It is worth following in some detail the nature of these products, as they are a representative benchmark for the reactivity of copper-bearing mixed catalysts through the pathways schematized in Fig. 4. Hydrogenolysis of the C-O bond of vanillic alcohol led to the formation of creosol. The hydrogenolysis of the C-O bond of BMBAlcohol led to the formation of a 4-benzyloxy-3-methoxytoluene (BMT) intermediate, which gave rise to 1-benzyloxy-2-methoxybenzene (BMB) through hydrogenolysis of the C-C bond between the methyl group and the aromatic ring. Vanillic alcohol and toluene were formed by hydrogenolysis of the α-O-4 phenolic ether bond.

The Fe_2O_3 catalyst was less active that both NiO and CuO catalysts, despite its higher surface area, 38 m^2 g-1 vs. 24 and 13 m^2 g^{-1} for, respectively, NiO and CuO (table S3). The main product was always BMBAlcohol from MPV reaction, albeit in amount lower than observed in the blank tests. Minor amounts of products from both transetherification and hydrogenation reactions were observed, indicating a reactivity including limited formation of products already observed on NiO as well as on CuO catalysts (Table S5). The carbon balance was 96%, slightly lower than the 100% carbon balance observed on NiO and CuO.

3.4.3. Cu-Ni-Fe catalysts

The conversion to individual products on the catalysts of the Cu-Ni-Fe system are reported in Table S6. The yields of the main products of the different types of reactions are reported in Fig. 6, together with conversion and carbon balance values. Conversion and distribution of products were strongly affected by the composition of the catalysts.

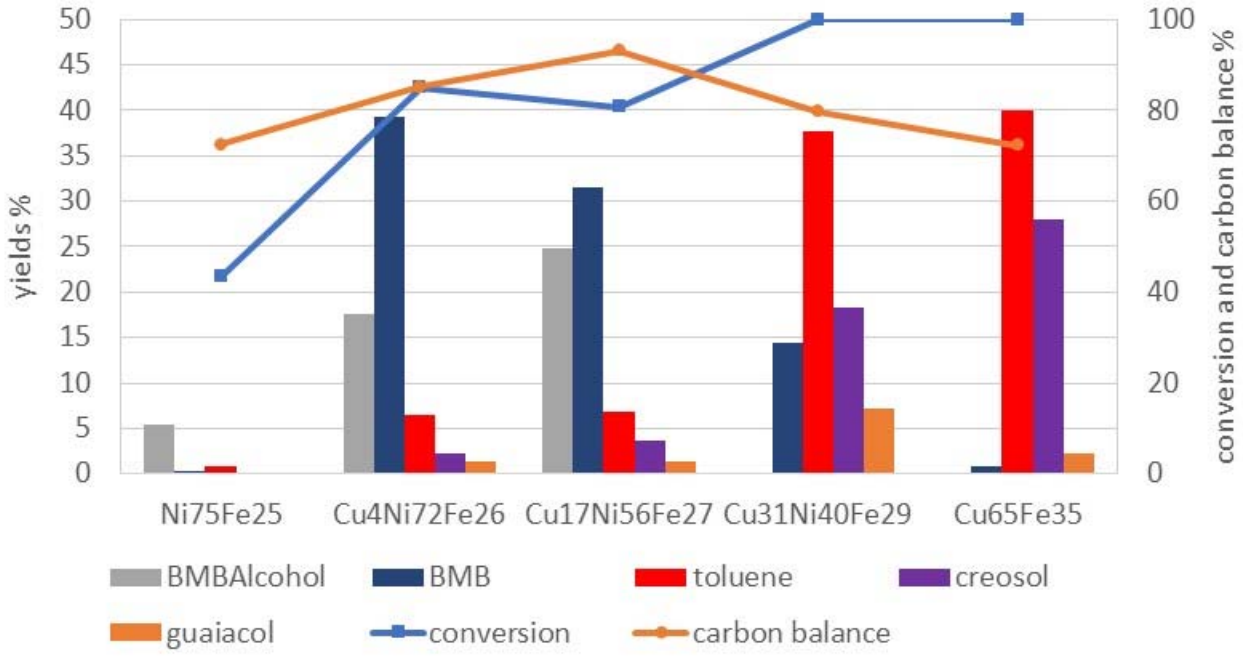

Fig. 6. Conversion, carbon balance and yields of main products of MPV hydrogenation (BMBAlcohol and BMB) and hydrogenolysis of α-O-4 (toluene, creosol and guaiacol), C-O (BMB, creosol and guaiacol) and C-C (BMB and guaiacol) bonds on catalysts of the Ni-Cu-Fe series.

The Cu-free Ni75Fe25 catalyst allowed a 43% conversion of BMBA, nearly twice the conversion observed on the pure NiO catalyst. This higher activity could be related to a higher surface area and smaller NiO crystallite size of the mixed catalyst, surface area being 89 m^2 g^{-1} for Ni75Fe25 vs. 24 m^2 g^{-1} for NiO, Scherrer crystallite size being 7 nm for Ni75Fe25 vs. 21 nm for NiO. However, the carbon balance of 72% was quite poor, indicating that nearly 60% of converted BMBA went into unidentified heavy condensation products and the conversion to identified products was not higher than 15%. The yield of BMBAlcohol, formed by MPV hydrogen exchange, was lower than 6% and further hydrogenation was nearly absent, the yield of α-O-4 hydrogenolyis products being about 1%. The cleavage of the α-O-4 bond mainly followed a transetherification pathway, with a 3% yield of veratraldehyde and 3.4% yield of benzylalcohol and its methyl ether. These low yields, nearly half the values observed on NiO, suggest that condensation of oxygenates may significantly contribute to the low carbon balance. At variance with NiO, some BMBAcetal was also formed (2.6% yield).

The introduction of copper in the catalyst critically increased the conversion of BMBA by comparison with the Cu-free catalyst. The replacement of 5% Ni by Cu in the Cu4Ni72Fe24

catalyst increased the conversion from 43 to 85%, improved the carbon balance from 72 to 85% and completely changed the distribution of products. The total yield of MPV hydrogenation of aldehydes was higher than 60% and further hydrogenation reactions converted most of the alcohols formed (Tab. S6 and Fig. 6). Only traces of BMT (4-benzyloxy-3-methoxy toluene), the C-O hydrogenolysis product of BMBAlcohol, were observed, as this reaction intermediate was nearly completely converted to BMB (1-benzyloxy-2-methoxy benzene), the product of C-C hydrogenolysis.

Another effect of the introduction of copper in the catalyst was the formation of products of hydrogenolysis of the α-O-4 bond with a yield of about 12%. Nearly no free vanillin was analysed. It was either completely converted to vanillic alcohol or bypassed in the chain of reactions of Fig. 6, vanillic alcohol being formed in majority by α-O-4 hydrogenolysis of BMBAlcohol, itself formed by a fast MPV hydrogenation of BMBA. Most vanillic alcohol was converted to products of C-O and C-C hydrogenolysis. However, the distributions of hydrogenolysis products from BMBAlcohol and vanillic alcohol did differ. If BMT is nearly completely converted to BMB, only about one third of creosol is hydrogenated to guaiacol, indicating that the reactivity of toluene-like C-C bonds was much higher in heavier oligomers than in lighter monomers.

At variance with what was observed on NiO, the products of transetherification of benzyl alcohol by methanol were in negligible amount. It is clear that the introduction of a limited amount of copper has completely altered the pattern of reactivity of the Ni-Fe catalyst, despite Ni being still, by a large extent, the majority cation. Globally, the pattern of activity of Cu4Ni72Fe24 parallels the product distribution observed on CuO, integrated by a strong enhancement of the hydrogenation behavior.

Increasing the amount of copper in the catalyst from Cu4Ni72Fe24 to Cu17Ni56Fe27 brought limited changes of the activity pattern, albeit the carbon balance was improved up to 93%. It can be observed that CuO tenorite phase, absent in Cu4Ni72Fe24, was still a minor phase in Cu17Ni56Fe27. When CuO became the main phase present, with further increase of the amount of copper to Cu31Ni40Fe29, the distribution of products was significantly modified. The global yield of products of MPV hydrogen transfer and their derivatives decreased from more than 60 to nearly 40% (Tab. S6 and Fig. 6). This decrease did not correspond to a decrease of activity, as the BMBA conversion was nearly 100%, but was due to a severe worsening of the carbon balance, decreasing to 80%, corresponding to the formation of non-analysed heavy products. At the same time, the yield of products of α-O-4 hydrogenolysis rose from 14% to nearly 65%. Among these products, the yield of toluene approached 38%. Vanillic alcohol was

in negligible amount and the cumulated yields of its hydrogenolysis products, creosol and guaiacol were less than 26% (Fig. 7). These values indicate a deficit of observed products issued from the vanillic half of the BMBA molecule, suggesting that condensation of oxygenates contributed to the formation of non-analysed heavy products.

As already observed at lower copper content, less than one third of creosol was hydrogenated to guaiacol, corresponding to a yield of C-C hydrogenolysis products significantly lower than the yield of C-O hydrogenolysis. BMBA which did not underwent cleavage of the α-O-4 bond was, instead, nearly completely hydrogenated to BMB, confirming a higher C-C cleavage activity for heavier molecules. No more BMBAcetal was observed, the large conversion of BMBA to hydrogenated products shifting back the equilibrium of the acetalisation reactions.

Further increase of the copper content brought to a significant worsening of the carbon balance. At complete substitution of nickel by copper, the Cu65Fe35 catalyst featured 100% conversion and 72% carbon balance (see Fig. 6). Only 1% of identified products retained an α-O-4 bond (see Table S6). The yield of toluene was 40%. This yield, as all yields in this work, is calculated on a carbon atom basis. As the 7 carbon atoms of toluene represent nearly 47% of the carbon atoms of BMBA, the yield of toluene on Cu65Fe35 reaches 85% of the maximum theoretical yield. This is not the case for the products of hydrogenation of intermediate vanillic alcohol, which present a 31% yield compared to a maximum theoretical yield of 53%. This confirms that a significant pathway to unidentified heavy products passes through condensation reactions of vanillic alcohol.

The decrease of the yield of products of MPV hydrogenation at high copper content (Fig. 6) is worth of remark. Indeed, unreacted aldehydes are not observed in the products and their acetals are in negligible amount (Table S6). This indicates by default that the MPV activity is extremely high and the decrease of MPV-derived products has to be attributed to competitive reactions. Indeed, the condensation of the aldehyde group of BMBA is the most likely pathway for the formation of heavy non-analysed products and the corresponding worsening of the carbon balance.

3.4.4. Cu-Ni-Al catalysts

Conversion of BMBA, carbon balance and yields of main products on the Cu-Ni-Al catalysts are shown in Fig. 7. Complete data are reported in Table S7. In the case of the Cu-free Ni75Al25 catalyst, the conversion is 20% and the carbon balance close to 100%. These values strongly differ from the ones observed on Ni75Fe25, indicating a lower activity and a much better carbon balance for Al-bearing than for Fe-bearing catalysts. Indeed, the values of conversion and

carbon balance were nearly identical to the ones observed on NiO in the absence of aluminium (Fig. 5). However, the distributions of products were quite different in the two cases. In the presence of aluminium, the yield of products of α-O-4 cleavage by transetherification decreased from 13% to less than 2%, the products of hydrogenolysis increased from less than 1% to nearly 3%, and the main product, with 8% yield, was BMBAcetal, not observed on single-cation NiO. The yield of MPV reactions, around 10%, was similar for NiO and Ni75Al25 catalysts but the presence of aluminium introduced some activity of hydrogenolysis of BMBAlcohol to BMB.

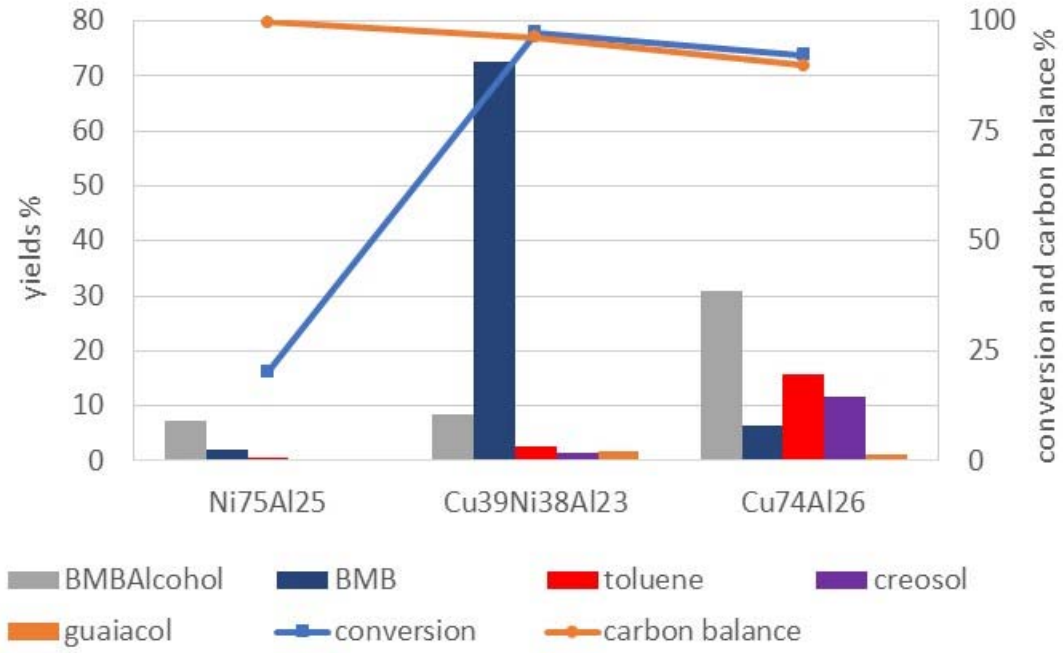

Fig. 7 . Conversion, carbon balance and yields of main products of MPV hydrogenation (BMBAlcohol and BMB) and hydrogenolysis of α-O-4 (toluene, creosol and guaiacol), C-O (BMB, creosol and guaiacol) and C-C (BMB and guaiacol) bonds on catalysts of the Ni-Cu-Al series.

The mixed copper-nickel Cu39Ni38Al23 catalyst presented 97% conversion and 96% carbon balance, being nearly as active as the corresponding iron-bearing Cu31Ni40Fe29 catalyst but presenting a much better carbon balance (compare Figs. 6 and 7). Their distributions of products were quite different. Whereas on the iron-bearing catalyst the products derived from hydrogenolysis of the α-O-4 presented a 63% yield, they reached only 8% yield on the aluminium-bearing catalyst. On the other hand, BMB, the product of total hydrogenation of the aldehyde group of BMBA, presented a yield of 72% on the aluminium-bearing catalyst *vs.* just

14% on the iron-bearing catalyst. Clearly, hydrogenation reactions beyond MPV hydrogen exchange were the predominant reactions on both Fe- and Al-bearing catalysts but the aluminium-bearing Cu39Ni38Al23 was much less effective in hydrogenolysis of the α-O-4 phenyl ether bond. Moreover, the observation on the Al-bearing catalyst of 8% yield of BMBAlcohol, the MPV primary product, negligible on the Fe-bearing catalyst, suggests a lower activity of hydrogenolysis of the C-O bond. The observation of a 4% yield of BMBAcetal is again suggestive of a significant acidity of the Al-bearing catalysts.

The Ni-free Cu74Al26 catalyst was less active (92% conversion) than the mixed Cu39Ni38Al23 and presented a poorer 90% carbon balance. The distribution of products was also very different. The higher yield of toluene (16%) and creosol (12%) corresponded to a higher activity of α-O-4 hydrogenolysis (see fig. 7). However, the significant amounts of BMBAlcohol (31% conversion) and vanillylmethylether (4% conversion), intermediate hydrogenation products, indicated that the hydrogenation activity of the Ni-free Cu74Al26 catalyst was lower than the one of the Ni- and Cu-bearing Cu39Ni38Al23. The significant yield of BMBAcetal (12%) can be attributed both to a significant acidity of the catalyst and to a higher availability of the BMB reagent due to its lower consumption by hydrogenation reactions.

3.5. Evaluation of the catalysis results

The reactions underwent by BMBA in the presence of different oxide catalysts correspond to different kinds of methanol activation. Methanol is the direct hydrogenation agent in the hydrogen exchange with aldehyde groups by MPV mechanism, whereas hydrogen formed by methanol reforming is the likely agent of hydrogenolysis of C-O, C-C and phenyl ether bonds. Methanol is also directly involved in benzyl-methyl transetherification, etherification of alcohol groups and acetalisation of aldehydes.

Among these reactions, hydrogenation reactions provide the main contribution to the conversion of the BMBA model molecule on the studied catalysts. The yields of MPV hydrogenation and hydrogenolysis of α-O-4, C-O and C-C bonds are reported in figure 8 for representative catalysts of the Cu-Ni-Fe and Cu-Ni-Al series and for single-cation nickel and copper oxides. In order to highlight the activity for each kind of reaction, the yields indicated in this figure are cumulative yields, including also the products of reactions consecutive to the reaction indicated. As an example, the cumulative yield of MPV reaction in Fig. 8 is the sum of the yields of BMBAlcohol and of all products of the consecutive reactions of BMBAlcohol as identified in Fig. 4.

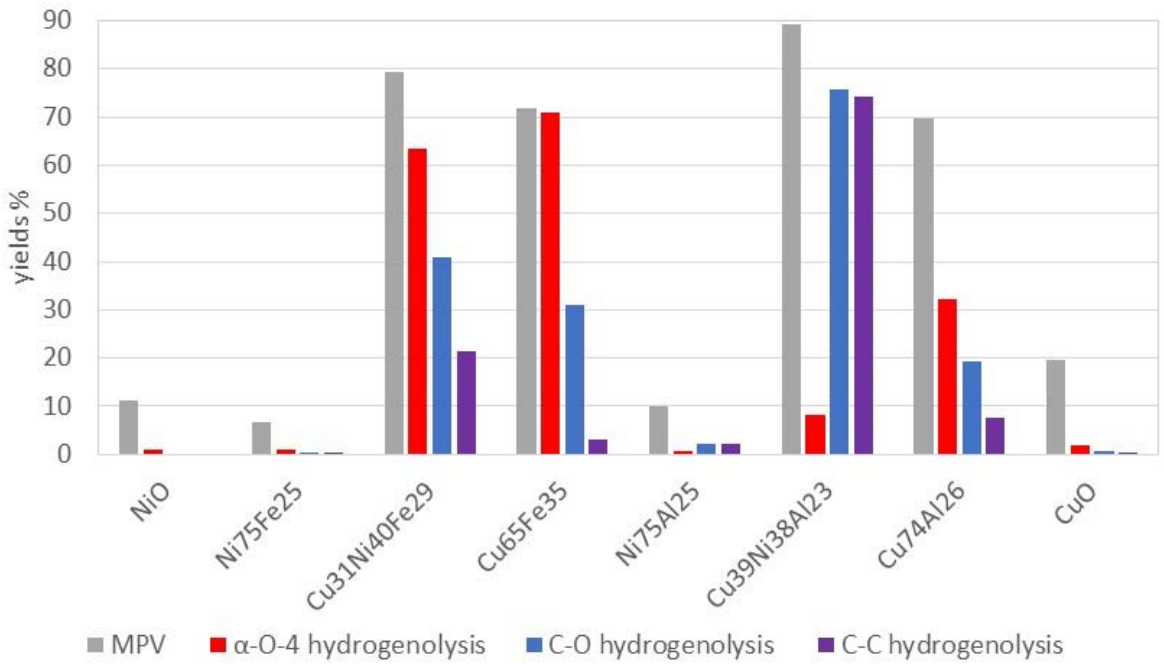

Fig. 8. Yields of products of hydrogenation reactions on representative catalysts.

It is apparent that single-cation NiO and CuO, as well as mixed oxides in the absence of copper, present only a limited MPV activity and virtually no deeper hydrogenation activity. High MPV and hydrogenation activities are instead observed on all Cu-bearing mixed oxide catalysts.
A correlation can be observed between the general trend of hydrogenation reactions and the reducibility of the catalysts, as desumed from the H_2-TPR data of Fig. 3 and Table 1. Cu-bearing mixed oxide catalysts present an onset of reduction by H_2 at temperature in the 180-220 °C field, lower than the reduction temperature of either oxides without copper or pure CuO. This high reducibility suggests that methanol at 200 °C can induce the formation of reduced sites, active both in methanol reforming and hydrogenation reactions. Indeed, classical mechanisms of hydrogen transfer reactions suggest that plain MPV hydrogenation of carbonyls is favoured on acid-base pairs, whereas metal sites are needed for hydrogenolysis reactions [70, 71].[70,71] As an instance, Fe_3O_4 is an effective catalyst of MPV transfer hydrogenation of aldehydes by hydrogen-donor alcohols at temperature lower than 120 °C [72].[72] Cu/Fe_3O_4 catalysts can be obtained by a reduction treatment of $CuO\text{-}Fe_3O_4$ oxides. On these catalysts, methanol in liquid phase at 150 °C is able to react with 5-hydroxymethylfurfural not only by MPV hydrogenation to 2,5-bis hydroxymethylfurfural but also inducing C-O hydrogenolysis to methylfurfural [73].[73] The hydrogen needed for the hydrogenolysis reactions is provided from methanol reforming through methanol dehydrogenation to acetaldehyde [74].[74] Acetaldehyde is dimerized to methyl

formiate, which is disproportionated to CO_2 and CH_4 through a highly thermodynamically favoured mechanism, which has been well documented on basic oxides at temperatures as low as 160 °C [27, 75].[27,75]

In order to verify the hypothesis of reduction of Cu-bearing catalysts in methanol, powder X-ray diffraction was carried out as a preliminary characterization of used catalysts. XRD patterns of copper-free catalysts after the reaction showed the same phase distribution as the fresh catalysts. Cu-bearing catalysts, instead, underwent an observable conversion of CuO tenorite to reduced phases. The diffraction patterns of representative catalysts before and after reaction are reported in Fig. 9. In the case of single cation CuO catalyst (Fig. 9a), the catalytic reaction has led to the reduction of a very limited fraction (nearly 1%) of CuO tenorite to Cu_2O cuprite (Fig. 9b). In the course of the reaction, this catalyst has shown some MPV activity (17% yield) but a very limited activity for deeper hydrogenation (2% yield) (Tab. S5).

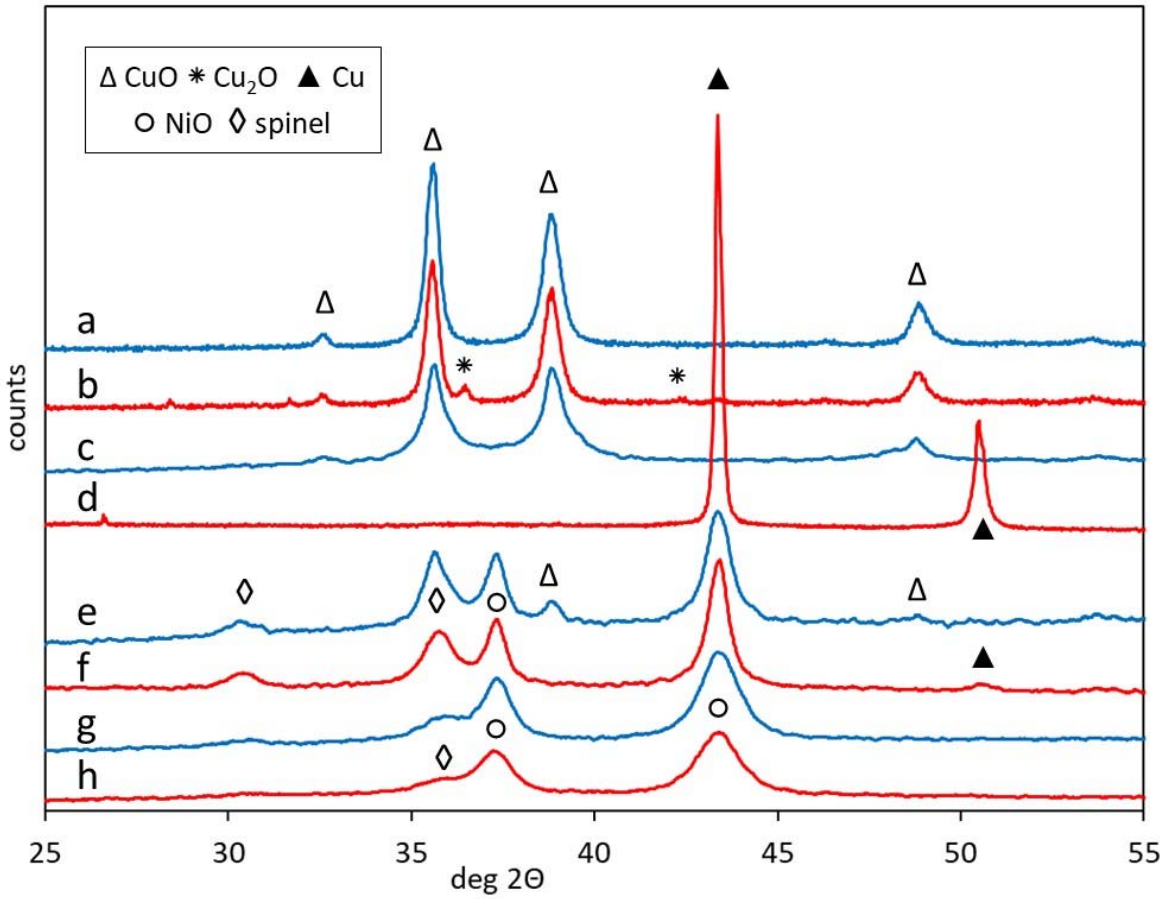

Fig. 9. XRD patterns of catalysts before and after conversion of BMBA in methanol, 200 °C, 3h. CuO fresh (a) and used (b). Cu74Al26 fresh (c) and used (d). Cu17Ni56Fe27 fresh (e) and used

(f), Ni75Fe25 fresh (g) and used (h). The counting of line 9D has been scaled down for sake of comparison.

Cu74Al26 catalyst (Fig. 9c), a much more effective hydrogenation catalyst, underwent a very severe reduction in methanol. After conversion of 92% BMBA, no more CuO tenorite diffraction lines are visible and metallic copper is the only crystalline phase observed (Fig. 9d). The diffraction patterns of Cu17Ni56Fe27 (Fig. 9e) also witness catalyst reduction after 80% conversion of BMBA (Fig. 9f). No modifications of NiO bunsenite and spinel phases are observable in the used catalyst. CuO tenorite diffraction lines, instead, have completely disappeared and have been replaced by the diffraction lines of metallic copper. It can be observed that catalysts from calcination of Cu-Mg-Al hydrotalcites were already reported to undergo some reduction when used in transfer hydrogenation from supercritical methanol [38].[38] An oxidation treatment brought back the catalyst to the initial oxidation state. However, it was later shown that this kind of catalysts did not present significant losses of activity when recycled without an intermediate oxidation treatment [76].[76]

In the case of Ni75Fe25, a copper-free catalyst providing 43% BMBA conversion but just 6% yield of reduction products (Table S6), no significant difference are observed between the diffraction patterns of the fresh (Fig. 9g) and used (Fig. 9h) catalyst. The stability of NiO bunsenite in our reaction conditions was responsible for a level of hydrogenation activity much lower than the one reported on reduced nickel catalysts [37].[37]

The reduction of CuO by methanol at 200 °C in liquid phase seems at least as effective as the reduction by H_2 in the TPR experiments in gas phase. It seems reasonable to assume that metallic copper formed in the reaction media is the most effective catalyst for hydrogenation and reforming reactions in this system. Understandably, the in-situ formation of active sites in the presence of reducing agents is more and more taken in due account in recent literature [77, 78].[77,78]

Both MPV hydrogen exchange and deeper hydrogenation are favoured on the highly reducible mixed oxide catalysts. However, the ratios between different hydrogenation reactions are affected by the composition of the catalyst. Just a cursory look at fig. 8 evidences that α-O-4 hydrogenolysis is much more effective in the iron-bearing than in the Al-bearing catalysts. This trend is correlated to other effects of the nature of the catalyst. In figure 10, the yield of α-O-4 hydrogenolysis products is compared with the methanol etherification activity and the carbon deficit, *viz*. the complement to unit of the carbon balance. The etherification activity is somehow difficult to quantify, as most of the alcohol groups formed by MPV reaction or solvolysis of the α-

O-4 bond are consumed by C-O hydrogenation. The choice made in Fig.10 is the representation of the etherification activity by the ratio between measured ethers and the sum of ethers and alcohols. It is clear that the formation of methyl ethers is increased by the presence of iron in the same way in which α-O-4 hydrogenolysis is. It is worth to observe that this effect of iron is strongly enhanced by the presence of copper, as shown by the weak etherification activity and the absence of α-O-4 hydrogenolysis on the copper-free Ni75Fe25 catalyst. It can also be observed that etherification by methanol is observed on alcohol groups and not on the phenolic hydroxils formed by α-O-4 hydrogenolysis.

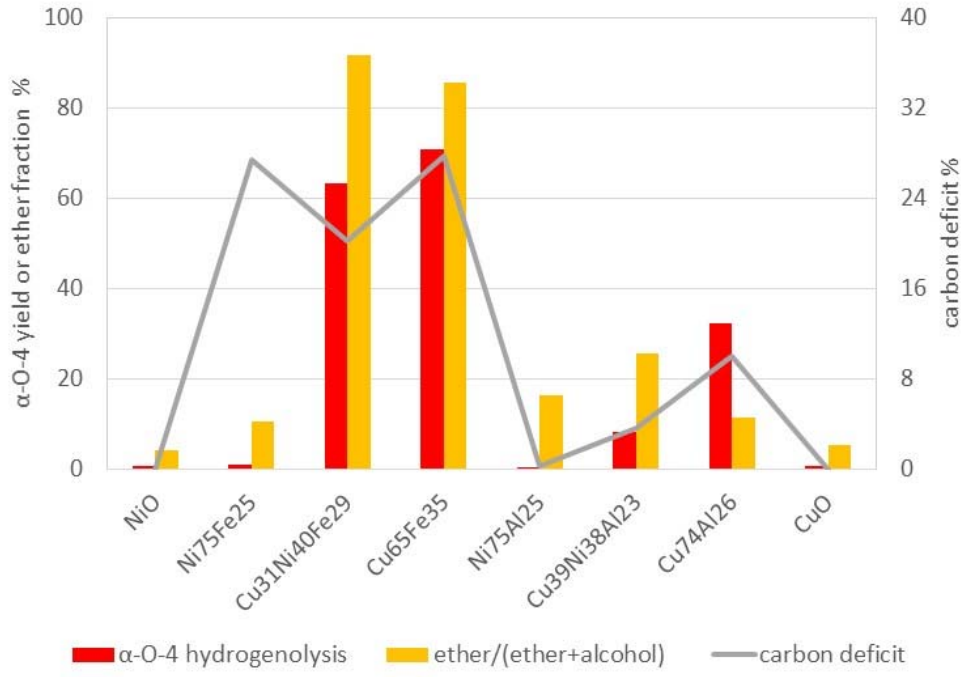

Fig. 10. Yield of products of α-O-4 hydrogenolysis, ether/(ether+alcohol) ratio and carbon deficit on representative catalysts.

Another effect of the presence of iron is the increase of the carbon deficit. This effect, mainly to be attributed to condensation of BMBA through its aldehyde group, is predominant in all Fe-bearing catalysts, also in the absence of copper. It can be remembered that, as observed in section 3.4.3, another contribution to the formation of heavy non-analysed compounds is related to the reactivity of vanillic alcohol, as inferred by the unbalance between the vanillic alcohol-derived products and the toluene formed by α-O-4 hydrogenolysis.

The composition of catalysts also affects, as already remarked, the ratio between C-O and C-C hydrogenolysis. It can be observed in Fig. 8 that, for very weak α-O-4 hydrogenolysis (see

catalyst Cu39Ni38Al23), the yields of C-O and C-C hydrogenolysis are equivalent, viz. nearly all products of C-O hydrogenolysis are further converted by C-C hydrogenolysis. For important α-O-4 hydrogenolysis, instead, the yield of C-C hydrogenolysis is much lower than the yield of C-O hydrogenolysis, indicating that a significant fraction of C-O hydrogenolysis products is no further hydrogenated. This corresponds to a much easier reducibility of the C-C bond for the BMT dimer than for monomeric creosol.

It can be also observed that no products of opening of the aromatic ring have been observed. This differ from the results of other studies and it can be questioned if the stability of the ring is due to milder temperature and pressure conditions or to the use of magnesium-free less alkaline catalysts in this study. It has been remarked that the absence of hydrogenation of the aromatic rings is a basic requirement for the processes aiming at the fine-chemistry valorisation of phenolic monomers [25].[25]

The methoxy groups of BMBA showed a remarkable stability in all products, quite a logical effect if the methanol excess in the reaction system is taken into account.

A minor contribution to the activity of the catalysts is brought by reactions not implying hydrogenation steps. Yields of acetalisation and transetherification products on representative catalysts are reported in Fig. 11. The data have to be examined by taking into account the competition with hydrogenation reactions, hence differentiating catalysts with low hydrogenation activity, like single-cation oxides, from mixed oxide catalysts with high hydrogenation activity. In the case of single-cation oxides, when faster hydrogenation reactions are not competing for reagents, CuO is very active in acetalisation and NiO is the best catalyst for phenyl-methyl exchange. In the case of mixed oxide catalysts, with strong competition by hydrogenation reactions, both these secondary reactions are prevented in the iron-bearing catalyst, whereas Al-bearing mixed oxides are effective acetalisation catalysts, probably due to the presence of acid sites of amorphous alumina. Cu-bearing mixed oxides from the calcination of MgAl hydrotalcite have been reported as effective acetalisation catalysts of acetaldehyde [79].[79] This effect has been attributed to the presence of strong acid sites, which have been shown to be virtually absent in calcined MgFe hydrotalcites [80].[80] It can be remarked that the formation of acetals has been proposed as an effective method to preserve oxygenated groups of lignin fragments for the production of epoxy resin monomers [81].[81]

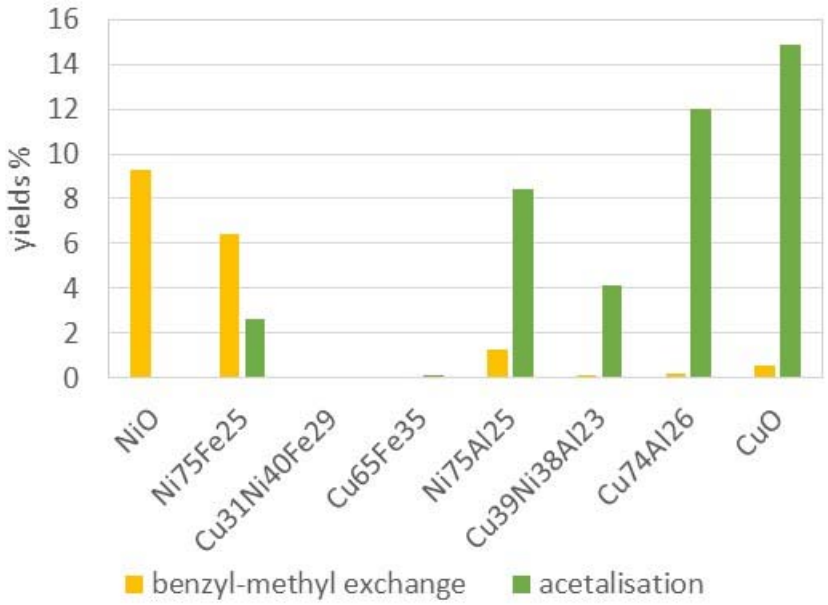

Fig. 11. Yield of products of acetalisation and benzyl-methyl transetherification on representative catalysts

4. Conclusions

Testing the hydrodeoxygenation of a lignin model by methanol in conditions of temperature and pressure similar to the ones of organosolv pulping processes allowed to highlight the role that mixed oxide catalysts can play in hydrogen transfer and further hydrogenation of lignin.

The reactivity of methanol with the lignin model in the absence of a catalyst was limited to a weak acetalisation activity. Nickel- and iron-bearing oxides present some activity in MPV hydrogen transfer. Nevertheless, iron-based catalysts poorly fare about another key topic of pulping: relevant formation of heavy products from condensation of lignin.

The presence of copper in the catalyst is critical for hydrogenation reactions, whose yield is increased by an order of magnitude. The preparation of copper-bearing catalysts by calcination of LDH with different cation composition allows tuning the activity of the catalyst both in MPV reaction and further hydrogenation reactions. The enhancement of the reducibility of CuO by the preparation of catalysts in the presence of NiO has a paramount importance in the increase of hydrogenation activity. Indeed, CuO can be reduced in-situ by methanol to metallic copper in the reaction conditions, forming supported metal active sites for methanol activation and hydrogenation reactions. The aromatic rings of liquid products are not affected by hydrogenation in these conditions, allowing the formation of high added-value phenolic compounds.

The need of an in-situ activation of catalyst for effective hydrogenation reactions introduces specific constraints to the reaction systems. The hydrogen-donor activity of the solvent is critical, either by direct exchange of by in-situ hydrogen generation, and a strict control of the redox environment of the system is required. The absence of strong acid or basic functions in the catalysts has allowed to isolate the effect of hydrogenation from other kinds of reactivity. The level of cleavage of phenolic ether bonds by the Cu-Al catalysts is indeed quite low. This strongly suggests that depolymerisation of lignin is unlikely to be improved by catalyst-triggered hydrogen transfer from a donor solvent alone. Very likely, organosolv delignification will continue to rely on acid-catalysed hydrolysis in the future. However, the hydrodeoxygenation of the lignin fraction by catalysed hydrogen transfer seems to be a viable improvement of the economy of organosolv processes. Heterogeneous catalysis clearly can play a role in the integration of organosolv pulping in biorefineries for the formation of valuable aromatics.

Acknowledgments

This work was supported by the SINCHEM Joint Doctorate programme selected under the Erasmus Mundus Action 1 Programme (FPA 2013-0037).

References

[1] A. J. Ragauskas, G. T. Beckham, M. J. Biddy, R. Chandra, F. Chen, M. F. Davis, B. H. Davison, R. A. Dixon, P. Gilna, M. Keller, P. Langan, A. K. Naskar, J. N. Saddler, T. J. Tschaplinski, G. A. Tuskan, C. E. Wyman, Lignin Valorization: Improving Lignin Processing in the Biorefinery. Science 2014, **344**, 1246843. DOI:10.1126/science.1246843.

[2] P. Lanzafame, G. Centi, S. Perathoner, Evolving scenarios for biorefineries and the impact on catalysis, Catal. Today 2014, 234, 2-12. DOI: 10.1016/j.cattod.2014.03.022.

[3] D. Esposito, M. Antonietti, Redefining biorefinery: the search for unconventional building blocks for materials, *Chem. Soc. Rev.*, 2015, **44**, 5821-5835. DOI: 10.1039/c4cs00368c.

[4] Z. Sun, B, Fridrich, A. Santi, S. Elangovan, K. Barta, Bright side of lignin depolymerization: Toward new platform chemicals. *Chem. Rev*. 2018, **118**, 614−678. DOI: 10.1021/acs.chemrev.7b00588

[5] R. Rinaldi, R. T. Woodward, P. Ferrini, H. J. E. Riverac, Lignin-First Biorefining of Lignocellulose: the Impact of Process Severity on the Uniformity of Lignin Oil Composition, *J. Braz. Chem. Soc.* 2019, **30**, 479-491. DOI: 10.21577/0103-5053.20180231.

[6] Y. Liao, S.-F. Koelewijn, G. Van den Bossche, J. Van Aelst, S. Van den Bosch, T. Renders, K. Navare, T. Nicolaï, K. Van Aelst, M. Maesen, I. Matsushima, J. M. Thevelein, K. Van Acker, B. Lagrain, D. Verboekend1, B. F. Sels. A sustainable wood biorefinery for low–carbon footprint chemicals production. *Science* 2020, **367**, 1385–1390. DOI: 10.1126/science.aau1567

[7] P. P. Thoresen, L. Matsakas, U. Rova, P. Christakopoulos, Recent advances in organosolv fractionation: Towards biomass fractionation technology of the future, *Bioresour. Technol*. 2020, **306**, 123189. DOI: 10.1016/j.biortech.2020.123189.

[8] X. Pan, C. Arato, N. Gilkes, D. Gregg,, W. Mabee, K. Pye, Z. Xiao, X. Zhang, J. Saddler, Biorefining of Softwoods Using Ethanol Organosolv Pulping: Preliminary Evaluation of Process Streams for Manufacture of Fuel-Grade Ethanol and Co-Products. *Biotech. Bioeng*. 2005, **90**, 473-481. DOI: 10.1002/bit.20453.

[9] J. Wildschut, A. T. Smit, Johannes H. Reith, Wouter J.J. Huijgen Ethanol-based organosolv fractionation of wheat straw for the production of lignin and enzymatically digestible cellulose. B*iores. Technol*. 2013, **135**, 58–66. DOI:10.1016/j.biortech.2012.10.050.

[10] Z. Zhang, M. D. Harrison, D. W. Rackemann, W. O. S. Doherty, I. M. O'Hara, Organosolv pretreatment of plant biomass for enhanced enzymatic saccharification, *Green Chem*., 2016, **18**, 360-381. DOI: 10.1039/c5gc02034d.

[11] S. Constant, A. Barakat, F. Di Renzo, M. Robitzer, C. Dumas, F. Quignard, Composition, texture and methane potential of cellulosic residues from Lewis acids organosolv pulping of wheat straw, B*iores. Technol*. 2016, **216**, 737-743. DOI: 10.1016/j.biortech.2016.06.019.

[12] O. Bobleter, Hydrothermal degradation of polymers derived from plants, *Prog. Polym. Sci*. 1994, 1**9**, 797–841. DOI: 10.1016/0079-6700(94)90033-7.

[13] S. Constant, M. Robitzer, F. Quignard, F. Di Renzo, Vanillin oligomerization as a model of side reactions in lignin fragmentation. *Catal.Today* 2012, **189**, 123-128. doi: 10.1016/j.cattod.2012.03.056.

[14] T. Renders, S. Van den Bosch, S.-F. Koelewijn, W. Schutyser, B. F. Sels, Lignin-first biomass fractionation: the advent of active stabilisation strategies, *Energy Environ. Sci.* 2017, 10, 1551-1557. DOI: 10.1039/c7ee01298e.

[15] J. Gierer. Chemistry of delignification Part 1: General concept and reactions during pulping. *Wood Sci. Technol.* 1985, **19**, 289-312. DOI: 10.1007/BF00350807.

[16] J. Gierer, I. Noren, S. Wännström. Formation of Condensation Products on Treatment of Non-Phenolic Lignin Units of the ß-Aryl Ether Type with Alkali. Model Studies on a Novel Mode of Alkaline Lignin Condensation. *Holzforschung* 1987, **41**, 79-82. DOI: 10.1515/hfsg.1987.41.2.79.

[17] P.J. Deuss, M. Scott, F. Tran, N. J. Westwood, J. G. de Vries, K. Barta. Aromatic Monomers by in Situ Conversion of Reactive Intermediates in the Acid-Catalyzed Depolymerization of Lignin. *J. Am. Chem. Soc*. 2015, **137**, 7456-7467. DOI: 10.1021/jacs.5b03693.

[18] V. M. Roberts, V. Stein, T. Reiner, A. Lemonidou, X. Li, A. Lercher, Towards Quantitative Catalytic Lignin Depolymerization, *Chem. Eur. J.* 2011, **17**, 5939-5948. DOI: 10.1002/chem.201002438.

[19] T. Voitl, P. R. von Rohr. Oxidation of Lignin Using Aqueous Polyoxometalates in the Presence of Alcohols. *ChemSusChem* 2008, **1**, 763-769. DOI: 10.1002/cssc.200800050.

[20] P. J. Deuss, C. W. Lahive, C. S. Lancefield, N. J. Westwood, P. C. J. Kamer, K. Barta, J. G. de Vries. Metal Triflates for the Production of Aromatics from Lignin. *ChemSusChem* 2016, **9**, 2974-2981. DOI: 10.1002/cssc.201600831.

[21] R.N. Olcese, M. Bettahar, D. Petitjean, B. Malaman, F. Giovanella, A. Dufour. Gas-phase hydrodeoxygenation of guaiacol over Fe/SiO2 catalyst. *Appl. Catal. B-Environ*. 2012, **115– 116**, 63-73. DOI:10.1016/j.apcatb.2011.12.005.

[22] T. M. Huynh, U. Armbruster, A. Martin, Deoxygenation of Liquid and Liquefied Biomass, in F. Cavani, S. Albonetti, F. Basile, A. Gandini (Eds.), *Chemicals and Fuels from Bio-Based Building Blocks*, Wiley 2016, pp. 403-429, DOI: 10.1002/9783527698202.ch16.

[23] E. Ranzi, P. E. Amaral Debiagi, A. Frassoldati, Mathematical Modeling of Fast Biomass Pyrolysis and Bio-Oil Formation. Note I: Kinetic Mechanism of Biomass Pyrolysis, ACS Sustainable Chem. Eng. 2017, **5**, 2867−2881. DOI: 10.1021/acssuschemeng.6b03096.

[24] X.-D. Fan, Y.-J. Wu, Z.-Y. Li, Y. Sun, R. Tu, P.-D. Zhong, E.-C. Jiang, X.-W. Xu. Benzene, toluene and xylene (BTX) from in-situ gas phase hydrodeoxygenation of guaiacol with liquid hydrogen donor over bifunctional non-noble-metal zeolite catalysts. *Renew. Energy* 2020, **152**, 1391-1402. DOI:10.1016/j.renene.2020.01.015.

[25] A.-L. Marshall, P. J. Alaimo. Useful Products from Complex Starting Materials: Common Chemicals from Biomass Feedstocks. *Chem. Eur. J*. 2010, **16**, 4970-4980. DOI: 10.1002/chem.200903028.

[26] M. Asadieraghi, W. M. A. Wan Daud, In-situ catalytic upgrading of biomass pyrolysis vapor: Co-feeding with methanol in a multi-zone fixed bed reactor, *Energy Convers. Manag.* 2015, **92**, 448–458. DOI: 10.1016/j.enconman.2014.12.082

[27] T. Pasini, A. Lolli, S. Albonetti, F. Cavani, M. Mella, Methanol as a clean and efficient H-transfer reactant for carbonyl reduction: Scope, limitations, and reaction mechanism, *J. Catal.* 2014, **317**, 206–219. DOI: 10.1016/j.jcat.2014.06.023.

[28] R. Rinaldi, F. Schüth, Design of solid catalysts for the conversion of biomass, *Energy Environ. Sci.*, 2009, **2**, 610-626. DOI: 10.1039/b902668a.

[29] R. Palkovits, K. Tajvidi, A. M. Ruppert, J. Procelewska, Heteropoly acids as efficient acid catalysts in the one-step conversion of cellulose to sugar alcohols, *Chem. Commun.,* 2011, **47**, 576-578. DOI: 10.1039/c0cc02263b.

[30] M. Yabushita, H. Kobayashi, A. Fukuoka, Catalytic transformation of cellulose into platform chemicals, *Appl. Catal. B-Environ*. 2014, **145**, 1-9. DOI: 10.1016/j.apcatb.2013.01.052.
[31] G. Gliozzi, A. Innorta, A. Mancini, R. Bortolo, C. Perego, M. Ricci, F. Cavani, Zr/P/O catalyst for the direct acid chemo-hydrolysis of non-pretreated microcrystalline cellulose and softwood sawdust, *Appl. Catal. B-Environ*. 2014, **145**, 24-33.
[32] R. Behling, S. Valange, G. Chatel, Heterogeneous catalytic oxidation for lignin valorization into valuable chemicals: what results? What limitations? What trends? *Green Chem.* 2016, **18**, 1839–1854. DOI: 10.1039/c5gc03061g
[33] A. Pineda, A.F. Lee, Heterogeneously catalyzed lignin depolymerization, *Appl. Petrochem. Res*. 2016, **6**, 243–256. DOI 10.1007/s13203-016-0157-y
[34] P. Sudarsanam, R. Zhong, S. Van den Bosch, S. M. Coman, V. I. Parvulescu, B. F. Sels. Functionalised heterogeneous catalysts for sustainable biomass valorization. *Chem. Soc. Rev*. 2018, **47**, 8349-8402. DOI: 10.1039/c8cs00410b.
[35] I. Z. Awan, N. Tanchoux, F. Quignard, S. Albonetti, F. Cavani, F. Di Renzo, Heterogeneous Catalysis as a Tool for Production of Aromatic Compounds From Lignin, in S. Albonetti, S. Perathoner, E. A. Quadrelli (Eds.), *Horizons in Sustainable Industrial Chemistry and Catalysis*, Elsevier 2019, pp. 257-275, DOI: 10.1016/B978-0-444-64127-4.00013-6.
[36] X. Wang, R. Rinaldi, Exploiting H-transfer reactions with RANEY® Ni for upgrade of phenolic and aromatic biorefinery feeds under unusual, low-severity conditions, *Energy Environ. Sci.*, 2012, **5**, 8244-8260. DOI: 10.1039/c2ee21855k.
[37] Q. Song, F. Wang, J. Cai, Y. Wang, J. Zhang, W. Yua, J. Xu, Lignin depolymerization (LDP) in alcohol over nickel-based catalysts via a fragmentation–hydrogenolysis process, *Energy Environ. Sci.*, 2013, **6**, 994-1007. DOI: 10.1039/c2ee23741e
[38] G. S. Macala, T. D. Matson, C. L. Johnson, R. S. Lewis, A. V. Iretskii, P.C. Ford, Hydrogen Transfer from Supercritical Methanol over a Solid Base Catalyst: A Model for Lignin Depolymerization, *ChemSusChem*, 2009, **2**, 215-217. DOI: 10.1002/cssc.200900033
[39] K. Barta, T. D. Matson, M. L. Fettig, S. L. Scott, A. V. Iretskii, P. C. Ford, Catalytic disassembly of an organosolv lignin via hydrogen transfer from supercritical methanol, *Green Chemistry*, 2010, **12**, 1640–1647. DOI: 10.1039/c0gc00181c.
[40] C. M. Bernt, H. Manesewan, M. Chui, M. Boscolo, P. C. Ford, Temperature Tuning the Catalytic Reactivity of Cu-Doped Porous Metal Oxides with Lignin Models, *ACS Sustainable Chemistry & Engineering,* 2018, **6**, 2510-2516. DOI: 10.1021/acssuschemeng.7b03969.
[41] T. D. Matson,K. Barta, A. V. Iretskii, P. C. Ford. One-Pot Catalytic Conversion of Cellulose and of Woody Biomass Solids to Liquid Fuels. *J. Am. Chem. Soc.* 2011, **133**, 14090–14097. DOI: 10.1021/ja205436c.
[42] T. S. Hansen, K. Barta, P.T. Anastas, P.C. Ford, A. Riisager. One-pot reduction of 5-hydroxymethylfurfural via hydrogen transfer from supercritical methanol. *Green Chem*., 2012, **14**, 2457-2461. DOI: 10.1039/c2gc35667h.
[43] J. Zhang, J. Chen, Selective Transfer Hydrogenation of Biomass-Based Furfural and 5-Hydroxymethylfurfural over Hydrotalcite-Derived Copper Catalysts Using Methanol as a Hydrogen Donor, *ACS Sustainable Chem. Eng*. 2017, **5**, 5982-5993, DOI: 10.1021/acssuschemeng.7b00778.
[44] Z. Sun, A. Couto Vasconcelos, G. Bottari, M. C. A. Stuart, G. Bonura, C. Cannilla, F. Frusteri, K. Barta. Efficient Catalytic Conversion of Ethanol to 1-Butanol via the Guerbet Reaction over Copper- and Nickel-Doped Porous. *ACS Sustain. Chem. Eng.* 2017, **5**, 1738−1746. DOI: 10.1021/acssuschemeng.6b02494..
[45] Z. Sun, D. Buwalda, K. Barta. Two-step catalytic conversion of lignocellulose to alkanes. RSC Adv., 2019, 9, 23727–23734. DOI: 10.1039/c9ra03174j.
[46] A. K. Deepa, P. L. Dhepe, Lignin Depolymerization into Aromatic Monomers over Solid Acid Catalysts, *ACS Catal.* 2015, **5**, 365−379, DOI: 10.1021/cs501371q.
[47] Y. Jiang, Z. Li, X. Tang, Y. Sun, X. Zeng, S. Liu, L. Lin, Depolymerization of Cellulolytic Enzyme Lignin for the Production of Monomeric Phenols over Raney Ni and Acidic Zeolite Catalysts, *Energy Fuels* 2015, **29**, 1662−1668, DOI: 10.1021/ef5022297.
[48] S. Van den Bosch, T. Renders, S. Kennis, S.-F. Koelewijn, G. Van den Bossche, T. Vangeel, A. Deneyer, D. Depuydt, C. M. Courtin, J. M. Thevelein, W. Schutyser, B. F. Sels, Integrating lignin valorization and bio-ethanol production: on the role of Ni-Al2O3 catalyst pellets during lignin-first fractionation, Green Chem., 2017, 19, 3313-3326, DOI: 10.1039/c7gc01324h.

[49] A. Johansson, O. Aaltonen, P. Ylinen, Organosolv Pulping-Methods and Pulp Properties, *Biomass*, 1987, **13**, 45-65. DOI: 10.1016/0144-4565(87)90071-0
[50] M. Zhou, B. K. Sharma, P. Liu, H. Xia, J. Xu, J.-C. Jiang, Microwave Assisted Depolymerization of Alkaline Lignin over Hydrotalcite-Based CuNiAl Mixed Oxides, *ACS Sustainable Chem. Eng*. 2018, **6**, 11519−11528. DOI: 10.1021/acssuschemeng.8b01697.
[51] J. Huang, C. Zhao, F. Lu, High-Efficient and Recyclable Magnetic Separable Catalyst for Catalytic Hydrogenolysis of α-O-4 Linkage in Lignin, *Polymers* 2018, **10**, 1077, DOI:10.3390/polym10101077.
[52] Z. B. Shifrina, L. M. Bronstein, Magnetically Recoverable Catalysts: Beyond Magnetic Separation, *Front. Chem.* 2018, **6**, 298. DOI: 10.3389/fchem.2018.00298.
[53] A.C. Larson, R.B. Von Dreele, General Structure Analysis System (GSAS), Los Alamos National Laboratory Report LAUR 86-748 (2000).
[54] B. H. Toby. EXPGUI, a graphical user interface for GSAS. *J. Appl. Cryst.* 2001, **34**, 210-213. DOI: 10.1107/S0021889801002242.
[55] R.J. Hill, C.J. Howard. Quantitative Phase Analysis from Neutron Powder Diffraction Data Using the Rietveid Method. *J. Appl. Cryst.* 1987, **20**, 467-474. DOI: 10.1107/S002188988708619
[56] D. L. Bish, S. A. Howard. Quantitative phase analysis using the Rietveld method. *J. Appl. Cryst.* 1988, **21**, 86-91. DOI: 10.1107/S0021889887009415.
[57] A.F. Gualtieri. A guided training exercise of quantitative phase analysis using EXPGUI (2003). GSAS Tutorials and Examples. http://www.cristal.org/DU-SDPD/nexus/ccp14/web/solution/gsas/gsastuto.htm.
[58] A.V. Neimark, P.I. Ravikovitch, Capillary condensation in MMS and pore structure characterization, *Micropor. Mesopor. Mat*. 2001, **44**, 697-707. DOI: 10.1016/S1387-1811(01)00251-7.
[59] R. J. Hill, J. R. Craig, G.V. Gibbs, Systematics of the Spinel Structure Type. *Phys. Chem. Minerals* 1979, **4**, 317-339. DOI: 10.1007/BF00307535.
[60] A. M. Balagurov, I. A. Bobrikov, M. S. Maschenko, D. Sangaa, V. G. Simkin, Structural Phase Transition in $CuFe_2O_4$ Spinel. *Crystallogr. Rep.* 2013, **58**, 710-717. DOI: 10.1134/S1063774513040044.
[61] B. Lavina, G. Salviulo, A. Della Giusta. Cation distribution and structure modelling of spinel solid solurtions. *Phys. Chem. Minerals* 2002, **29**, 10-18. DOI: 10.1007/s002690100198.
[62] H. D. Colorado, G. A. Pérez Alcázar. Magnetic and structural properties of Cu0.85Fe0.15O system synthesized by co-precipitation. *Hyperfine Interact*. 2011, **202**, 139–144. DOI: 10.1007/s10751-011-0354-0.
[63] F. Trifirò, A. Vaccari, O. Clause, Nature and properties of nickel-containing mixed oxides obtained from hydrotalcite-type anionic clays, *Catal. Today* 1994, **21**, 185-195. DOI: 10.1016/0920-5861(94)80043-X.
[64] V. Rives, S. Kannan, Layered double hydroxides with the hydrotalcite-type structure containing Cu^{2+}, Ni^{2+} and Al^{3+}, *J. Mater. Chem.* 2000, 1**0**, 489-495. DOI: 10.1039/a908534c.
[65] J. Sa´, Y. Kayser, C. J. Milne, D. L. Abreu Fernandes, J. Szlachetko, Temperature-programmed reduction of NiO nanoparticles followed by time-resolved RIXS, *Physical Chemistry Chemical Physics*, 2014, **16**, 7692-7696. DOI: 10.1039/C3CP54622E.
[66] Y.-S. Jung, W.-L. Yoon, Y.-S. Seo, Y.-W. Rhee, The effect of precipitants on Ni-Al2O3 catalysts prepared by a co-precipitation method for internal reforming in molten carbonate fuel cells, *Catalysis Communications*, 2012, 2**6**, 103-111. DOI:10.1016/j.catcom.2012.04.029.
[67] A. Khan, P. Chen, P. Boolchand, P. G. Smirniotis Modified nano-crystalline ferrites for high-temperature WGS membrane reactor applications,, *Journal of Catalysis*, 2008, 91-104. DOI: 10.1016/j.jcat.2007.10.018.
[68] O. Vozniuk, C. Bazzo, S. Albonetti, N. Tanchoux, F. Bosselet, J.-M. M. Millet, F. Di Renzo, F. Cavani, Structural changes of binary/ternary spinel oxides during ethanol anaerobic decomposition, C*hemCatChem*, 2017, **9**, 2219-2230. DOI: 10.1002/cctc.201601605.
[69] Q.-C. Yu, A.-C. Zhang, B. Yang, Dispersion of copper oxide supported on γ-alumina and its sulfation properties, *Trans. Nonferrous Met. Soc. China*, 2011, **21**, 2644-2648. DOI: 10.1016/S1003-6326(11)61104-7.
[70] M. J. Gilkey, B. Xu, Heterogeneous Catalytic Transfer Hydrogenation as an Effective Pathway in Biomass Upgrading. *ACS Cata*l. 2016, **6**, 1420-1436, DOI: 10.1021/acscatal.5b02171.
[71] A. Lolli, Y. Zhang, F. Basile, F. Cavani, S. Albonetti, Beyond H2: Exploiting H-Transfer Reaction as a Tool for the Catalytic Reduction of Biomass, in F. Cavani, S. Albonetti, F. Basile, A. Gandini (Eds.), *Chemicals and Fuels from Bio-Based Building Blocks*, Wiley 2016, pp. 353-378, DOI: 10.1002/9783527698202.ch14.

[72] M. Ma, P. Hou, P. Zhang, J. Cao, H. Liu, H. Yue, G. Tian, S. Feng. Magnetic Fe_3O_4 nanoparticles as easily separable catalysts for efficient catalytic transfer hydrogenation of biomass-derived furfural to furfuryl alcohol. *Applied Catal. A. Gen.* 2020, 602, 117709. DOI: 10.1016/j.apcata.2020.117709.

[73] I. Elsayed, M. A. Jackson, E. B. Hassan. Hydrogen-Free Catalytic Reduction of Biomass-Derived 5-Hydroxymethylfurfural into 2,5-Bis(hydroxymethyl)furan Using Copper−Iron Oxides Bimetallic Nanocatalyst. *ACS Sustain. Chem. Eng*. 2020, **8**, 1774−1785. DOI: 10.1021/acssuschemeng.9b05575.

[74] V. Crocellà, G. Cerrato, G. Magnacca, C. Morterra, F. Cavani, S. Cocchi, S. Passeri, D. Scagliarini, C. Flego, C. Perego. The balance of acid, basic and redox sites in Mg/Me-mixed oxides: The effect on catalytic performance in the gas-phase alkylation of m-cresol with methanol. *J. Catal*. 2010, **270**, 125–135. DOI: 10.1016/j.jcat.2009.12.011.

[75] M. S. Gyngazova, L. Grazia, A. Lolli, G. Innocenti, T. Tabanelli, M. Mella, S. Albonetti, F. Cavani. Mechanistic insights into the catalytic transfer hydrogenation of furfural with methanol and alkaline earth oxides. *J. Catal*. 2019, **372**, 61-73. DOI: 10.1016/j.jcat.2019.02.020.

[76] Z. Sun, G. Bottari, A. Afanasenko, M. C. A. Stuart, P. J. Deuss, B. Fridrich, K. Barta1. Complete lignocellulose conversion with integrated catalyst recycling yielding valuable aromatics and fuels. *Nat. Catal*. 2018, **1**, 82–92 DOI: 10.1038/s41929-017-0007-z.

[77] N. Ballarini, F. Cavani, S. Passeri, L. Pesaresi, A. F. Lee, K. Wilson, Phenol methylation over nanoparticulate CoFe2O4 inverse spinel catalysts: The effect of morphology on catalytic performance *Applied Catalysis A: General*, 2009, **366,** 184-192. DOI:10.1016/j.apcata.2009.07.003.

[78] M. Ma, H.Liu, J. Cao, P. Hou, J. Huang, X. Xu, H. Yue, G. Tian, S. Feng, A highly efficient Cu/AlOOH catalyst obtained by in situ reduction: Catalytic transfer hydrogenation of ML into γ-GVL, *Mol. Catal.* 2019, **467**, 52–60. DOI: 10.1016/j.mcat.2019.01.033

[79] I.-C. Marcu, N. Tanchoux, F. Fajula, D. Tichit. Catalytic Conversion of Ethanol into Butanol over M–Mg–Al Mixed Oxide Catalysts (M = Pd, Ag, Mn, Fe, Cu, Sm, Yb) Obtained from LDH Precursors. *Catal. Lett*. 2013, **143**, 23–30. DOI: 10.1007/s10562-012-0935-9.

[80] M. León, E. Díaz, A. Vega, S. Ordóñez, A. Auroux. Consequences of the iron–aluminium exchange on the performance of hydrotalcite-derived mixed oxides for ethanol condensation. *Appl. Catal. B Environ*. 2011, **102**, 590–599. DOI:10.1016/j.apcatb.2010.12.044.

[81] A. Kaiho, D. Mazzarella, M. Satake, M. Kogo, R. Sakaia, T. Watanabe. Construction of the di(trimethylolpropane) cross linkage and the phenylnaphthalene structure coupled with selective β-O-4 bond cleavage for synthesizing lignin-based epoxy resins with a controlled glass transition temperature. *Green Chem.*, 2016, **18**, 6526–6535. DOI: 10.1039/c6gc02211a.